# 2nd Advanced Optical Metrology Compendium

## Advanced Optical Metrology

Geoscience | Corrosion | Particles | Additive
Manufacturing: Metallurgy, Cut Analysis & Porosity

EVIDENT
OLYMPUS

WILEY

**The latest eBook from Advanced Optical Metrology. Download for free.**

This compendium includes a collection of optical metrology papers, a repository of teaching materials, and instructions on how to publish scientific achievements.

With the aim of improving communication between fundamental research and industrial applications in the field of optical metrology we have collected and organized existing information and made it more accessible and useful for researchers and practitioners.

EVIDENT
OLYMPUS

WILEY

# 3D Microprinting of Super-Repellent Microstructures: Recent Developments, Challenges, and Opportunities

*Zheqin Dong\* and Pavel. A. Levkin\**

Liquid super-repellent surfaces, characterized by a low liquid–solid contact fraction, allow various liquids to bead up and freely roll off. Apart from liquid repellency, these surfaces feature several unique properties, including inter alia, self-cleaning, low-friction, anti-icing, and anti-biofouling, making them valuable for a vast array of applications involving liquids. Essential to achieve such super-repellency is the bio-inspired reentrant or doubly reentrant micro-topography. However, despite their unique interfacial properties, the fabrication of these delicate 3D topographies by conventional microfabrication methods is extremely challenging. Recently, emerging 3D microprinting technologies, particularly two-photon lithography, have brought new scope to this field. With unparalleled design freedom and flexibility, 3D microprinting greatly facilitates the design, testing, and studying of complex 3D microstructures. Here, applications of 3D microprinting in the design and fabrication of super-repellent microstructures are summarized, with a focus on their remarkable properties, and new functionalities offered by these intricate 3D topographies. Current challenges and new opportunities of emerging 3D microprinting techniques to further advance liquid super-repellent materials are also discussed.

## 1. Introduction

The development of functional materials has been playing an increasingly important role to advance science, technology, and our daily life. Among various material properties and functionalities, surface wettability is a crucial one that dictates the interaction of materials with liquids. Such liquid–solid interactions are ubiquitous in nature (e.g., wetting of plant leaves, insects, soils), as well as in our daily life (e.g., cooking, drinking) and industry (e.g., heat transfer, biomedical devices, submarine equipment). Thus, controlling the surface wettability of materials is important from both fundamental and application perspectives. Surfaces that display extreme liquid repellency, characterized by their large apparent liquid contact angle ($\theta^* > 150°$) and a small roll-off angle ($\alpha$) or contact angle hysteresis ($\Delta\theta^*$),[1–3] are especially interesting from the practical perspective but at the same time challenging to fabricate. These super-repellent surfaces feature unique properties, such as staying dry, self-cleaning,[4] low friction,[5] anti-icing,[6] and anti-biofouling,[7,8] making them valuable for applications ranging from electronic textile,[9] solar energy,[10] liquid transport,[11] aerospace,[12] to biomedical engineering.[13,14]

Interestingly, nature inspiration has played an indispensable role in the development of super-repellent surfaces.[15–17] A famous example is the amazing purity of lotus leaves, which has long been praised by many poets and artists. Until the 1990s, scientists revealed that such purification is attributed to the self-cleaning effect of the superhydrophobic surface, which, in turn, results from the synergetic effect of a high roughness and low surface energy.[18] This discovery ignited the interests of scientists from various fields (physics, chemistry, materials), and led to the explosive growth of the field of super-repellent surfaces in the past two decades (Figure S1, Supporting Information). To date, a variety of superhydrophobic coatings and materials have been developed by combining the effect of surface energy and roughness.[19–21] Despite excellent water repellency, these surfaces are, however, unable to repel organic liquids with relatively lower surface tensions (e.g., oils, alcohols).

To make surfaces super-repellent to a broad range of liquids (superoleophobic), scientists were inspired by the extreme water and oil resistance of springtails' skin.[22] It was demonstrated that reentrant or doubly reentrant (DRT) topography, is

Z. Dong
School and Hospital of Stomatology
Cheeloo College of Medicine Shandong University & Shandong Key
Laboratory of Oral Tissue Regeneration & Shandong Engineering
Laboratory for Dental Materials and Oral Tissue Regeneration
No. 44-1 Wenhuaxi Road, Jinan, Shandong 250012, China
E-mail: zheqindong@sdu.edu.cn
Z. Dong, Pavel. A. Levkin
Institute of Biological and Chemical Systems – Functional Molecular
Systems (IBCS-FMS)
Karlsruhe Institute of Technology (KIT)
Hermann-von-Helmholtz-Platz 1
76344 Eggenstein-Leopoldshafen, Germany
E-mail: levkin@kit.edu
Pavel. A. Levkin
Institute of Organic Chemistry (IOC)
Karlsruhe Institute of Technology (KIT)
Fritz-Haber Weg 6, 76131 Karlsruhe, Germany

**ADVANCED
SCIENCE NEWS**
www.advancedsciencenews.com

**ADVANCED
FUNCTIONAL
MATERIALS**
www.afm-journal.de

the key to achieving superoleophobicity.[23,24] Indeed, by using the DRT topography, surfaces that can repel liquids with very low surface tension (e.g., perfluorinated solvents or alkanes) have been realized.[25] More importantly, these studies changed the longstanding opinion that super-repellency requires hydrophobic/oleophobic materials, opening a new avenue to manipulate solid–liquid interactions by surface micro-structuring alone. Nevertheless, fabrication of such delicate 3D microstructures by using conventional techniques (e.g., photolithography, drying etching) is not trivial and laborious, requiring expensive devices and multiple steps.[25–27] In addition, the geometrical complexity of the produced 3D microstructures is quite limited. Therefore, further development of liquid super-repellent surfaces calls for advanced fabrication technologies with high design flexibility.

3D printing, also known as additive manufacturing, has been a driving force for the innovation and manufacturing of advanced materials in the past decade.[28–32] By assembling materials in a fully digital manner, 3D printing offers unparalleled design freedom and flexibility, opening a door to previously inaccessible material structures and properties. Although most 3D printing technologies are currently limited to submillimeter scale resolution, a few of them can fabricate objects with micrometer/submicrometer precision including electrohydrodynamic printing (EHDP),[33,34] electron-beam induced deposition (EBID),[35,36] projection micro-stereolithography (PµSL),[37,38] two-photon lithography (TPL),[39] and the newly developed two-step absorption (TSA) lithography.[40,41] Despite their relatively slower fabrication speed, these 3D microprinting techniques offer much higher flexibility in 3D geometrical design compared with conventional subtractive microfabrication methods (**Table 1**), making them attractive for the design and study of advanced liquid-repellent microstructures.

Among various 3D microprinting techniques, TPL has gained significant popularity during the past decade.[57–60] A key advantage of TPL lies in its ability to realize arbitrary geometry with a sub-micrometer resolution, which effectively facilitates the testing and studying of complex 3D microstructures. In addition, TPL allows the processing of diverse functional materials from polymer and ceramics to metals,[44] in contrast to traditional 3D microfabrication methods, such as dry etching or photolithography, relying on a few specialized materials (e.g., copper, silicon). Such versatility allows customization of the material property to meet the requirement of each specific application. With these unique advantages, TPL opens a new avenue to design and fabricate novel liquid super-repellent 3D microstructures previously inaccessible. Indeed, recent research in this direction has led to the development of super-repellent surfaces with enhanced performance and excitingly new functionalities (**Figure 1**).

In this review, we will discuss the recent developments, challenges, and opportunities in this emerging field. First, we analyze the key challenges to achieve liquid super-repellency from a fundamental viewpoint. Then, we highlight some representative novel microstructures enabled by TPL, which lead to enhanced liquid-repellent performances including low liquid adhesion, high impalement pressure, or side repellency. Next, we illustrate how the customizable material property offered by TPL can be leveraged to endow super-repellent surfaces with additional new functionalities including switchable repellency, gecko-like adhesion, or directional liquid transport. Finally, we provide an outlook on possible future research directions involving technology progress, material development, design strategies, and new applications.

## 2. Fundamental Challenges in the Fabrication of Liquid Super-Repellent Surfaces

When a liquid droplet contacts an ideally flat surface (**Figure 2**A), its equilibrium contact angle is determined by the balance of three surface tension forces: liquid–vapor, liquid–solid, and vapor–solid, as described in Young's equation[61]

$$\cos\theta_Y = \frac{\gamma_{sv} - \gamma_{sl}}{\gamma_{lv}} \tag{1}$$

where $\gamma$ refers to the interfacial tension and the subscripts $s$, $l$, and $v$ refer to the solid, liquid, and vapor phases, respectively.

**Table 1.** Comparison of different 3D microprinting methods and subtractive microfabrication methods in terms of fabrication rate, resolution, 3D design flexibility, and applicable materials.

| Categories | Method | Maximum resolution | Fabrication speed | 3D design flexibility | Applicable materials | Refs. |
|---|---|---|---|---|---|---|
| 3D microprinting | TPL | 50 nm | ★★★ | ★★★★★ | Polymer, metal, ceramics | [42–45] |
| | TSA | 150 nm | ★★★ | ★★★★★ | Polymer | [40,41] |
| | PµSL | 600 nm | ★★★★ | ★★★★ | Polymer, metal, ceramics | [37,38] |
| | EHDP | 80 nm | ★★ | ★★★ | Metal | [33,34] |
| | EBID | 10 nm | ★ | ★★★★ | Metal | [35,36] |
| Subtractive 3D microfabrication | LIGA | 50 nm | ★★★ | ★★ | Polymer, metal, ceramics | [46–48] |
| | RIE | 80 nm | ★★★ | ★ | Semiconductor, metal | [25,49,50] |
| | Micromilling | 10 µm | ★★★★★ | ★★★ | Metal, polymer | [51–53] |
| | PLA | 40 nm | ★★★★ | ★★★ | Metal, glass, polymer | [54–56] |

Abbreviations: Two-photon lithography (TPL); two-step absorption (TSA); projection microstereolithography (PµSL); electrohydrodynamic printing (EHDP); electron-beam-induced deposition (EBID); lithography, electrogrowth, moulding (LIGA); reactive ion etching (RIE); and pulse laser ablation (PLA). A qualitative comparison for build speed and design flexibility is provided, where more stars mean higher speed/flexibility and the same number of stars indicates similar speed/flexibility.
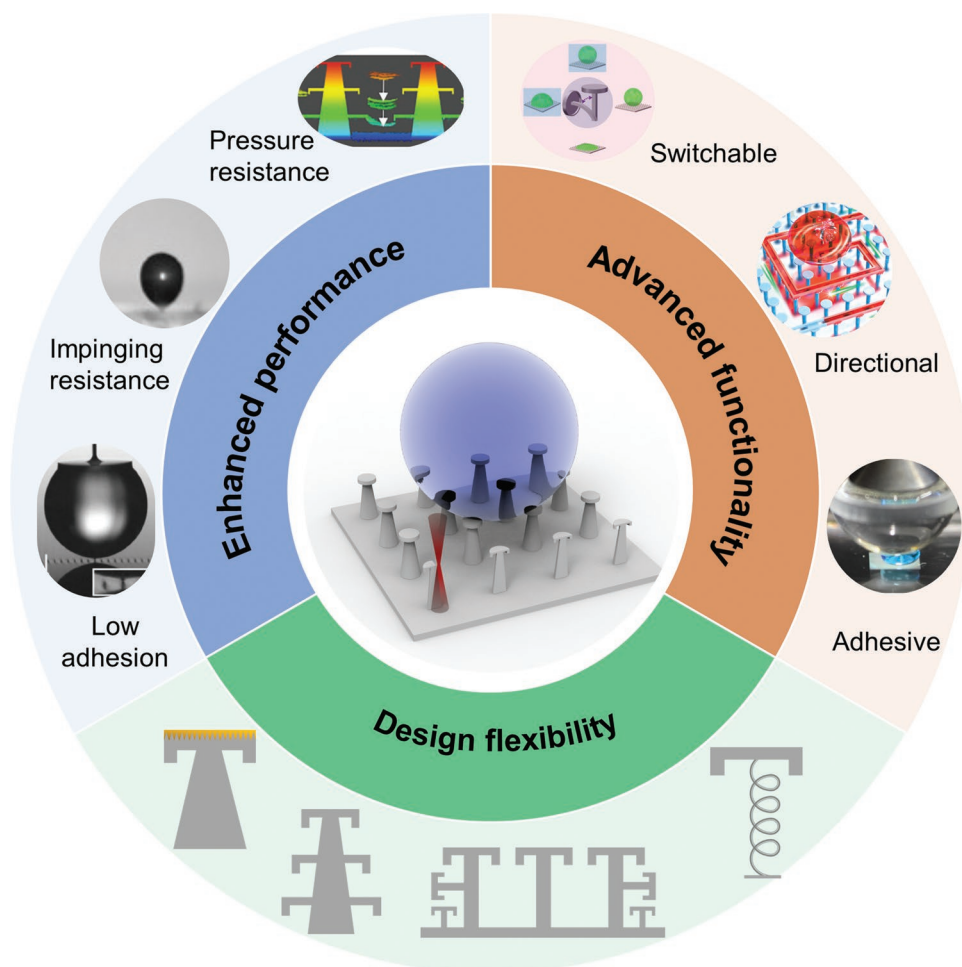
**Figure 1.** Overview of emerging applications of TPL in the design and manufacturing of super-repellent microstructures with enhanced performance and advanced functionalities.

The Young's contact angle $\theta_Y$ reflects the intrinsic wettability of material, therefore, it is also referred to as the intrinsic contact angle. As one can see from Equation (1), decreasing the surface energy of a solid should lead to an increase of $\theta_Y$, and therefore, should improve liquid repellency. However, even with the lowest surface energy of perfluorinated materials, the contact angle of the water ($\gamma = 72$ mN m$^{-1}$) on a flat surface does not exceed 120°,[62] not to mention most organic liquids with lower surface tensions. Thus, liquid super-repellency cannot be achieved by surface chemistry alone.

The contact angle of liquid drops on a rough surface can generally be described by two different models: Wenzel[63] and Cassie–Baxter[64] (i.e., Cassie for short) (Figure 2A). In the Wenzel model, the rough texture is fully wetted by a liquid and the apparent contact angle $\theta^*$ follows the following equation[63]

$$\cos\theta^* = r\cos\theta_Y \tag{2}$$

where the surface roughness factor $r$ is defined as the ratio of the actual to the projected surface area of the substrate.

In the Cassie state, on the other hand, the droplet is suspended by air pockets, resulting in a composite interface. The contact angle on such a composite interface can be calculated by averaging the value on air (i.e., 180°) and the solid (i.e., $\theta_Y$), which yields[64]

$$\cos\theta^* = -1 + f_s(1+\cos\theta_Y) \tag{3}$$

where $f_s$ is the liquid–solid contact fraction, that is, the proportion of liquid–solid contact area to the projected area of the entire composite interface.

Although it is possible to achieve a very high contact angle ($\theta^* > 150°$) in both Wenzel and Cassie states, the liquid adhesive property differs significantly.[65] In the Cassie state, the droplet sits partially on air with a small solid–liquid contact fraction, which minimizes the adhesion force as exemplified by their low sliding angle ($\alpha$) and contact angle hysteresis ($\Delta\theta^*$). For a Wenzel droplet, by contrast, the liquid–solid contact area is significantly higher, leading to the strong pinning effect. Therefore, to achieve super-repellency, it is essential to ensure the droplet stays in the Cassie state with a low solid–liquid contact.

From a thermodynamic perspective, the condition for which the Cassie state is preferred can be determined by comparing the Wenzel and Cassie equations[65]
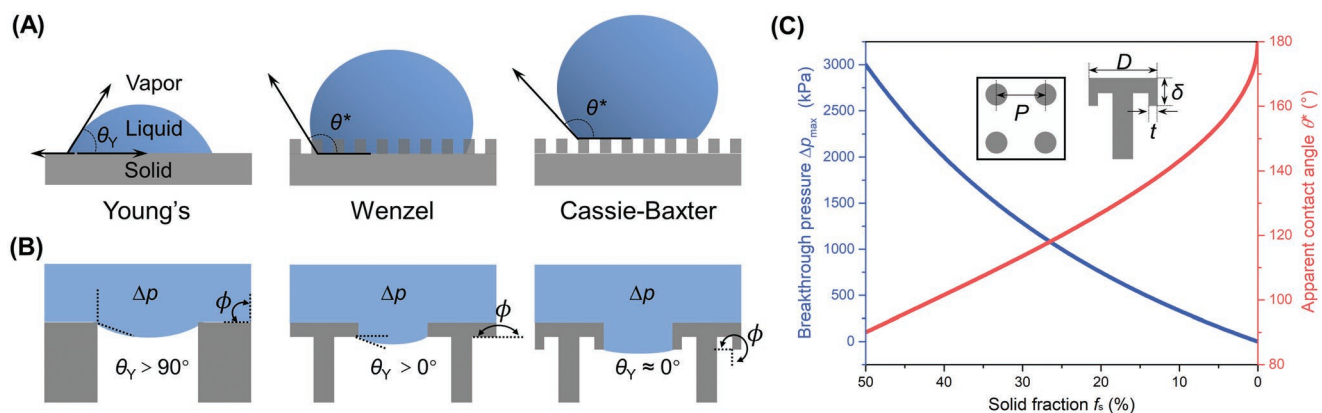
**Figure 2.** A) Schematic diagram showing different wetting models of a liquid droplet on a solid surface. B) Liquid suspension on microstructures of three different topographies: pillar ($\phi = 90°$) requires $\theta_Y > 90°$; reentrant ($\phi = 180°$) requires $\theta_Y > 0°$; and doubly reentrant ($\phi = 270°$) requires $\theta_Y \geq 0°$. C) Relation between breakthrough pressure ($\Delta p_{max}$), apparent contact angle ($\theta^*$), and solid fraction ($f_s$) for an idea DRT microstructure array. A schematic diagram of the DRT array is inserted, where the center-to-center distance ($P$), top cover diameter ($D$), cover height ($\delta$), and vertical overhang thickness ($\delta$) are marked. Assuming $D$ is fixed at 20 µm, and $\delta$ and $t$ are small enough to be negligible.

$$\cos\theta_Y < \frac{f_s - 1}{r - f_s} \tag{4}$$

Since $> 1 > f_s$, meeting this criterion requires Young's contact angle $\theta_Y$ to be larger than 90°. While this is possible for high surface tension liquids (e.g., water) by using low surface-energy substances, creating a material to realize $\theta_Y > 90°$ for liquids with relatively low surface tension (e.g., alkanes) is out of reach.

Alternatively, the Cassie state can be achieved by designing textures that create multiple local free energy minima, leading to so-called "metastable" configurations.[66] In this scenario, the well-defined local free energy minimum generates a kinetic barrier, which prevents the transition to the Wenzel state despite its global free energy minimum. A common strategy to design a metastable Cassie state is by exploiting the edge effect.[67] When a liquid invades a rough texture, the contact line will be pinned at the edge due to the boundary minimum of the free energy. The criterion for the contact line to cross the edge is defined as

$$\theta_c = \theta_Y + \phi > 180° \tag{5}$$

where $\phi$ is the edge angle of the microstructure and $\theta_Y$ is Young's contact angle.

Figure 2B compares the suspension of liquid on three different types of topographies: vertical pillar, reentrant, and DRT microstructures.[25] For simple pillar microstructures ($\phi = 90°$), $\theta_Y > 90°$ is always required to suspend the liquid, meaning they are unable to repel low surface tension liquids. On the other hand, reentrant ($\phi = 180°$) and DRT ($\phi = 270°$) topologies can theoretically suspend a liquid even with $\theta_Y > 0°$ and $\theta_Y \geq 0°$, respectively.

However, one should keep in mind that such a suspended state is only metastable and can readily transition to the energetically favorable Wenzel state. Considering a liquid with $\theta_Y < 90°$ on a (doubly) reentrant array, the breakthrough pressure ($\Delta p_{max}$) required to induce the Cassie-to-Wenzel transition can be described as follows[68]

$$\Delta p_{max} = \begin{cases} \dfrac{4\pi D}{4P^2 - \pi D^2}\gamma\sin\theta_Y & \phi = 180° \\[2mm] \dfrac{4\pi D}{4P^2 - \pi D^2}\gamma & \phi = 270° \end{cases} \tag{6}$$

where $D$ is the diameter of the top cover, $P$ is the center-to-center spacing, and $\gamma$ is the surface tension of the liquid.

As can be seen from Equation (6), DRT microstructures create a higher breakthrough pressure than their reentrant counterparts (because $\sin\theta_Y \leq 1$), and the effect is more pronounced with the decrease of intrinsic contact angle ($\theta_Y$). Therefore, DRT structure is always preferred for designing liquid super-repellent surfaces, especially when repellency to extremely low surface tension liquids is demanded.

Once the liquid is suspended, the liquid–solid contact fraction $f_s$ becomes a critical parameter. The decrease of $f_s$ not only increases the apparent contact angle ($\theta^*$) as can be deduced from Equation (3) but also significantly reduces the liquid adhesion (small $\Delta\theta^*$).[69–71] Hence, reducing solid contact is an efficient strategy to improve liquid repellency. This can be achieved by either decreasing pillar diameter ($D$) or by increasing the spacing between pillars ($P$). Decreasing pillar diameter is a preferred option, as the pillar spacing can be reduced at the same time to allow simultaneously improved breakthrough pressure ($\Delta p_{max}$) and reduced adhesion ($\Delta\theta^*$).[70] Indeed, reducing pillar diameter down to nanometer scale has been realized for superhydrophobic vertical structures (e.g., nanograss), leading to extremely small $f_s$ (≈0.01%) and low adhesion.[72,73] However, due to the limitations of current fabrication techniques, it is extremely difficult if not impossible to fabricate delicate DRT structures with feature sizes below the micrometer scale. Therefore, such a strategy is not suitable to apply for low surface tension liquids, yet.

Increasing the pillar spacing ($P$) can also reduce $f_s$, but inevitably leads to a decrease in the breakthrough pressure ($\Delta p_{max}$). Assuming the length and thickness of the double reentrant cover are small enough, then $f_s$ can be simplified as ($\pi D^2/4P^2$), which converts Equation (6) to

**ADVANCED
SCIENCE NEWS**

www.advancedsciencenews.com

**ADVANCED
FUNCTIONAL
MATERIALS**

www.afm-journal.de

$$\Delta p_{\max} = \frac{4\gamma}{D\left(\frac{1}{f_s}-1\right)} \tag{7}$$

Figure 2C shows the trend of $\theta^*$ and $\Delta p_{\max}$ as a function of $f_s$ at a fixed pillar top diameter. Clearly, in this scenario, there is an inherent trade-off between liquid repellency and pressure resistance. Indeed, it has been shown experimentally that with the decrease of DRT pillar spacing ($P$), $\Delta p_{\max}$ increases at the expense of increased Cassie adhesion due to the extended three-three-phase contact line.[74] Thus, the fabrication of super-repellent surfaces with both high liquid repellency and robust Cassie-state stability, while crucial for their practical applications, remains a highly challenging task.

## 3. Liquid Super-Repellent Microstructures with Enhanced Performance

As discussed earlier, improving the liquid-repellency of textured surfaces by simply decreasing $f_s$ sacrifices its pressure resistance and leads to the Cassie-to-Wenzel transition. Thus, advancing the properties/performance of liquid super-repellent surfaces calls for novel structural design that can circumvent this inherent trade-off relationship. However, conventional top-down methods (e.g., micromachining, drying etching) for fabricating liquid super-repellent microstructures are sophisticated and offer little 3D design freedom. On the other hand, bottom-up approaches, while simple and straightforward, are generally not controllable and often lead to stochastic micro/nanostructures lacking clearly defined geometrical features.[2,75–77]

TPL, an emerging technology for 3D microfabrication, has been progressively developed during the past decade.[43,78–80] Due to the nonlinearity of two-photo polymerization, TPL allows the fabrication of nearly arbitrary 3D microstructures with well-defined features down to the sub-micrometer scale. With such attributes, TPL offers new possibilities to design and fabricate microstructures with unparalleled geometrical complexity and freedom. In the following chapter, we will highlight a few representative novel liquid super-repellent microstructures enabled by TPL including slippery DRT, multi-layered DRT, spring-like DRT, and top and lateral integrated DRT structures. We show how these advanced structures break the trade-off relationship between repellency and stability, leading to substantially improved performance.

Besides decreasing $f_s$, an alternative approach to decrease liquid adhesion is by introducing a liquid–liquid interface instead of a solid–liquid one. Unlike solid surfaces which are coarse and chemically heterogeneous at the microscale, the dynamic nature of liquid ensures a defect-free and molecularly smooth interface, thus significantly reducing the pining/adhesion of the repelling liquids.[85] This idea has been realized and developed by locking a slippery lubricant into a porous substrate (SLIPS).[86–89] Indeed, such a SLIPS, despite its large liquid–liquid contact interface, demonstrates extremely low adhesion ($\Delta\theta^*$) toward liquids across a wide range of surface tension (17.2–72.4 mN m$^{-1}$). Inspired by this concept, Dong et al. proposed a novel slippery DRT microstructure, which combines

the properties of a composite Cassie-state interface with the ultrasmooth nature of SLIPS (**Figure 3**A).[81] This is realized by first using TPL to fabricate DRT micropillars with dedicated nanostructures on top, followed by infusing the nanostructures with lubricants. Indeed, by introducing a slippery layer on top, the DRT microstructures showed an evident decrease in the adhesion force and contact angle hysteresis toward water droplets; and the top nanostructures increased the stability of the liquid top layer. More importantly, such an ultrasmooth liquid interface also confers the slippery DRT microstructures with unique anti-biofouling, anti-icing, or anti-frosting properties, making them valuable for a broad range of applications.

Compared with static repellency, dynamic liquid repellency under external stimuli and vibration, or liquid impact, is more relevant and critical for real-life applications. Inspired by the stepwise wetting behavior of springtails, Sun et al. proposed a novel liquid-repellent microstructure design with multiple energy barriers (Figure 3B).[82] By using TPL, they fabricated tapered post arrays, where each post is made of multilayered, DRT overhangs with increasing diameter from top to bottom. Such a smart design decoupled the demands of static and dynamic liquid repellency on geometric features, enabling both high $\theta^*$ and a gradually increased $\Delta p_{\max}$ from top to bottom. The multi-layered microstructures feature stepwise pinning–sagging wetting characteristics as revealed by confocal microscopy, establishing a breakthrough pressure gradient. Dynamic liquid repellency tests show that the multi-layered overhangs were able to resist the impact of ethylene glycol droplets and ensure complete rebound at $We$ ($We = 2\rho^2 VR/\gamma$) number higher than 35, while liquid readily penetrated into the single-layered control surface when $We$ number reached 20 ($We = 2\rho^2 VR/\gamma$ where $\rho$ is the liquid density, $V$ is the impact velocity, and $R$ is the droplet radius). Furthermore, the robustness of the multi-layered topography was manifested by the prolonged lifetime of air cushions in submerged conditions, which is crucial for under-liquid applications.

Besides the topological features of textured surfaces, substrate flexibility also plays a critical role in liquid repellency.[90–92] Hu et al. proposed a strategy to enhance kinetic liquid repellency by constructing a flexible spring-like support underneath the repelling reentrant top cover (Figure 3C).[83] The microstructures were realized by TPL, and their kinetic resistance was then evaluated under liquid impact with increasing $We$ number. The mushroom-spring-like microstructures demonstrated a considerable increase in kinetic resistance (i.e., a 15% increase of the breakthrough $We$ number) in comparison to the control surface made of rigid mushroom pillars. In addition, the flexible-mushroom microstructures also showed a significant reduction of contact time during liquid impact, which is particularly valuable for anti-icing applications.[93,94] The improved performance can be attributed to the compression of flexible supports during liquid impinging, thus reducing the relative impacting velocity and force. However, since the flexible microstructures were still fabricated on a rigid substrate, the oscillation amplitude was small, limiting the performance improvement. By making the entire surface flexible, further enhancement of liquid repellency is anticipated.

Although DRT micropillars effectively prevent liquids penetration from the top, they are susceptible to lateral inhibition
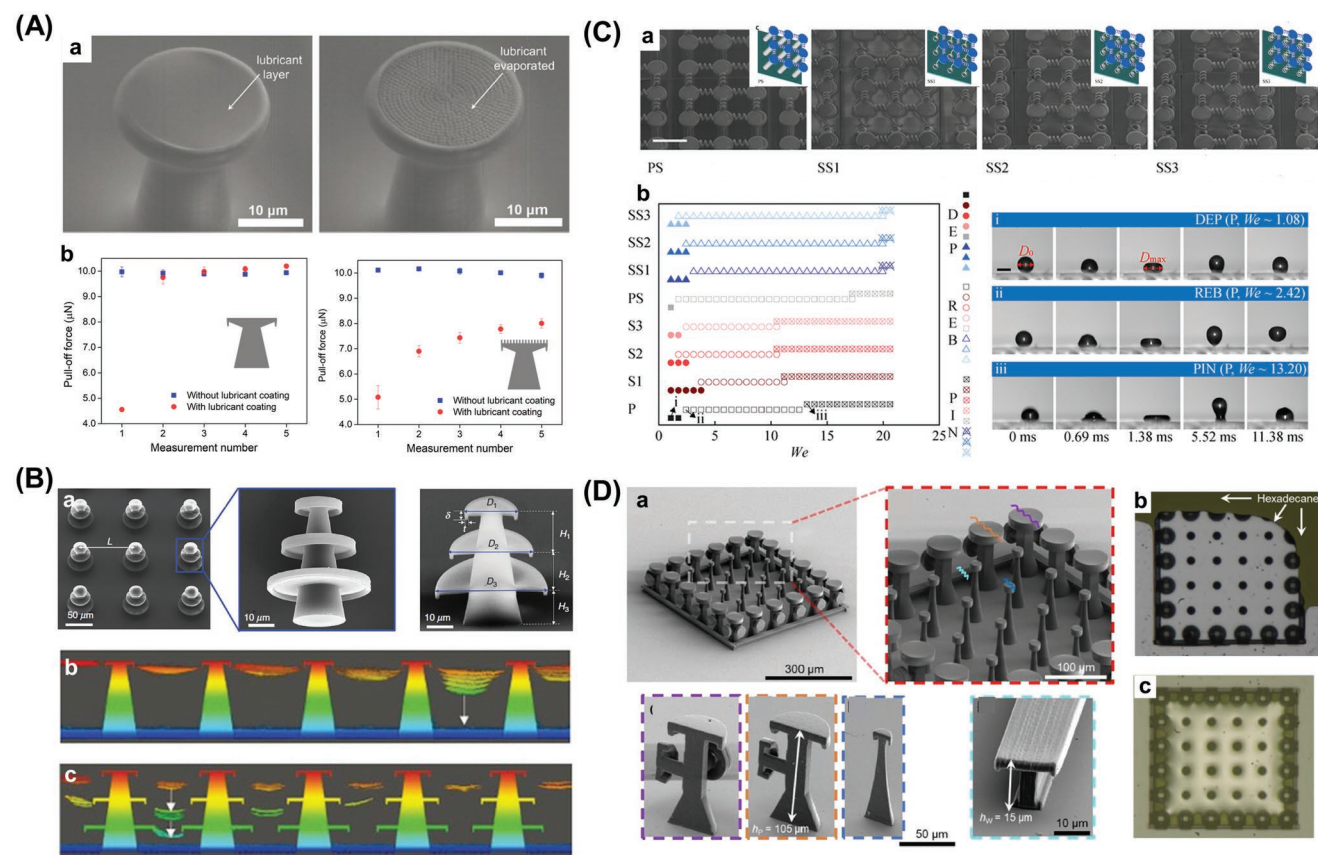
**ADVANCED**
**SCIENCE NEWS**
www.advancedsciencenews.com

**ADVANCED**
**FUNCTIONAL**
**MATERIALS**
www.afm-journal.de

**Figure 3.** Liquid super-repellent 3D microstructures with enhanced performance. A) Low liquid-adhesion slippery DRT microstructures. a) Environmental scanning electron microscope (SEM) images showing the lubricant oil layer covering the nanopillars on top of DRT microstructures. b) Pull-off forces on DRT microstructures with and without lubricant coating during five consecutive measurements: left, flat top; right, nanorough top. Reproduced with permission.[81] Copyright 2018, John Wiley and Sons. B) Pressure-resistant multilayered DRT microstructures. a) SEM images showing the multilayered, DRT overhangs. b) Confocal image showing the stepwise sagging of liquid–air interface on the multi-layered microstructures, while the liquid front gradually descends and finally collapses to the substrate for the single-layered control. Reproduced with permission.[82] Copyright 2021, American Institute of Physics. C) Impalement resistant flexible microstructures. a) SEM images of and (b,c) droplet impacting behavior on three mushroom-spring flexible surfaces with different numbers of active coils (SS1, SS2, and SS3) and a mushroom-pillar rigid surface (PS). Reproduced with permission.[83] Copyright 2020, American Association for Advancement Science. D) Side-repellent DRT microarray. a) SEM images showing the design: a DRT microarray surrounded by pillars with a mushroom-shaped cap both on the top and side, and a short wall with a DRT profile. b) Optical microscope images showing the entrapped air inside the 3D micro-texture when immersed under a hexadecane column of 5 mm height. Reproduced with permission.[84] Copyright 2020, Nature Publishing Group.

as the liquid can readily spread from the side to displace the trapped air. To enable side liquid-repellency, DRT cavity-based textures have been proposed.[26,27,95] While such architectures can improve the stability of entrapped air upon liquid immersion, their continuous solid–liquid-vapor three-phase contact line leads to the loss of liquid super-repellency (i.e., pinning).[71,96] To address this issue, Das et al. designed a DRT microarray surrounded by pillars with a mushroom-shaped cap both on the top and side, and a short wall with a DRT profile (Figure 3D).[84] As liquids impinging from the top hardly contact with the side caps and walls, their top repellency was maintained as proved by the measured high receding angles. On the other hand, the lateral microstructures robustly prevent the lateral invasion of liquids. Upon immersion in hexadecane, the DRT array with lateral caps and walls can entrap air pockets for more than 2 weeks, as opposed to the immediate liquid invading the control surface. Such an exceptional air-trapping ability makes these structures especially interesting

for long-term under-liquid applications. However, it should be pointed out that the strategy requires the intrinsic contact angles to be not too low ($\theta_Y > 40°$) in order to achieve a sufficient pinning force.

## 4. Liquid Super-Repellent Microstructures with Advanced Functionalities

In addition to its geometrical design freedom, another key advantage of TPL lies in the customizable material property,[44] by either adjusting the printing resin or writing parameters. Such a possibility adds a new dimension to the design of liquid super-repellent surfaces, allowing additional novel functionalities for wider applications. In what follows, we highlight how scientists combined the topological features of 3D microstructures with elaborately designed material properties offered by TPL to confer liquid-repellent materials with advanced

functionalities including switchable repellency, gecko-like adhesion, and directional liquid transport.

Switchable liquid-repellent surfaces which adapt to the surrounding environment are desirable for many fields including microfluidics,[99] sensors,[100] and liquid transportation[101] and separation.[102] Despite significant progress achieved in this field, reported surfaces are mostly applicable in air and to liquids with not too low surface tension ($\gamma > 25$ mN$^{-1}$). To allow switchable repellency for a broad range of liquids ($\gamma = 12$–72.8 mN m$^{-1}$), Liu et al. designed and printed deformable DRT microstructures using TPL (**Figure 4**A).[97] By controlling the laser power and scan speed, they deliberately adjusted the stiffness of the DRT microstructures to enable sufficient durability for suspending liquid droplets while allowing controllable deformation. During the evaporation of isopropanol,

the DRT microstructures bend toward the substrate due to capillary force, which changes the topological edge angle from 270° to 90° and significantly decreases the breakthrough pressure. As a result, liquid droplets can readily penetrate and spread on the bended microstructures. Indeed, the oil (*n*-hexadecane) in air, water in air, and oil underwater contact angles decrease from around 147°, 152°, and 153° to <5°, 95°, and 108°, respectively, indicating the loss of super-repellency. Similar trends were also observed when replacing *n*-hexadecane with various other liquids, including those with extremely low surface tension (perfluorooctane, $\gamma = 12$ mN m$^{-1}$). Furthermore, the bent microstructures can recovery by first immersing in a relatively good solvent (e.g., ethyl acetate) to release the residual stress, followed by drying in low surface tension and more volatile solvent (e.g., isopentane) to avoid evaporation-induced
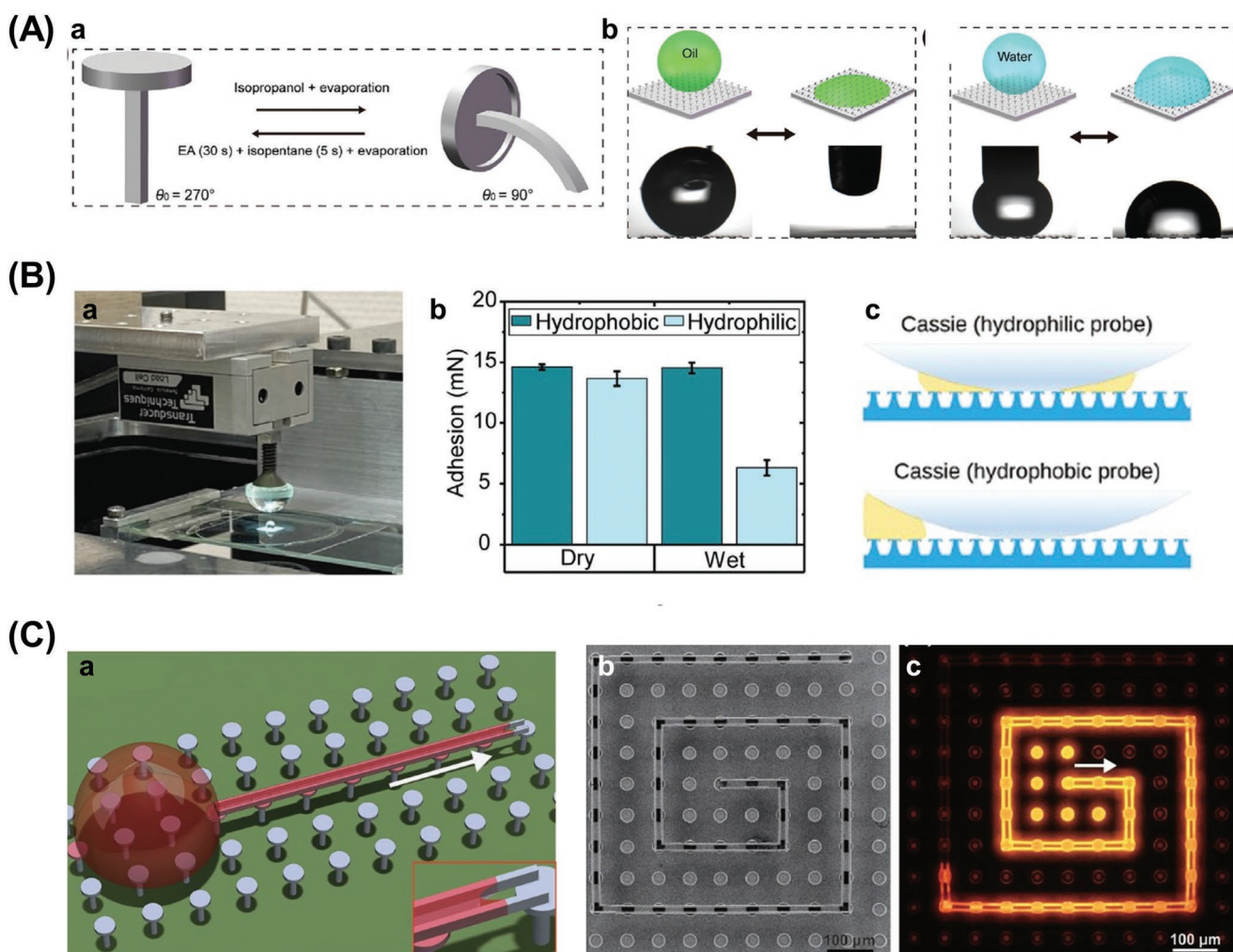


**Figure 4.** Liquid super-repellent 3D microstructures with advanced functionalities. A) Switchable super-repellent surfaces. a) Schematic illustration of the liquid-responsive bending and recovery of the DRT microstructures. b) Schematic diagrams and digital pictures showing the switchable repellency and spreading/penetration behaviors for oil and water in the air. Reproduced with permission.[97] Copyright 2020, John Wiley and Sons. B) Liquid super-repellent dry fibrillar adhesives. a) A photo showing the custom adhesion set-up with a liquid droplet on top of the sample. b) Dry and wet adhesion results using both hydrophobic and hydrophilic hemisphere glass probes. c) Schematic illustration of the measurement when liquid is present at the contact interface. Reproduced with permission.[98] Copyright 2021, John Wiley and Sons. C) Directional flow on super-repellent surfaces. a) Simulation figure shows the directional liquid flow on the triply re-entrant array with two parallel walls. b) SEM image of a microchannel constructed on the triply re-entrant array. c) Fluorescence image after the deposition and evaporation of a dyed ethanol droplet at the start of the capillary channel. Reproduced with permission.[68] Copyright 2018, John Wiley and Sons.

deformation. Thus, a reversible switch of liquid repellency can be achieved.

Gecko-inspired dry adhesives that can reversibly attach to diverse materials have become a vibrant research topic in the past decade.[103] While their fibrillar microstructure provides a strong adhesion in the dry state, the performance deteriorates in wet conditions due to a dramatic decrease in van der Waals forces. To address this issue, Liimatainen et al. designed a hybrid microstructure by combining the fibrillar feature of Gecko and the DRT topography of springtails, thus enabling both dry adhesion and liquid repellency (Figure 4B).[98] As dry adhesives require soft elastic structures for a compliant contact, they developed a custom-made resin based on the urethane-acrylate elastomer. Thanks to the elasticity and high surface energy (40.4 mN m$^{-1}$) of the customized material, the hybrid microstructures showed a high dry adhesive strength of 115 kPa, similar to those gecko-inspired adhesives reported in the literature. On the other hand, the DRT topography ensures liquid repellency even for highly wetting liquids (e.g., perfluorooctane). Therefore, if a hydrophobic probe is used in the wet adhesion test, the hybrid microstructure can repel liquid droplets away to establish a dry contact interface and maintain the high adhesive force. These results highlight the advantages of merging different concepts to achieve multiple functionalities at the same time.

Open microfluidics based on capillary flow finds broad applications in diagnostics,[104] analytical chemistry,[105] and biotechnology.[106] Typically, the liquid flow is confined in the channel by using geometrical boundary or wettability contrast, but these strategies are difficult to apply for low surface tension liquids due to their highly wetting nature. To enable the direction flow of various organic solvents in an open environment, Liu et al. first printed an array of triply reentrant microstructures, which possess the same high level of breakthrough pressure compared with DRT topography but are less sensitive to structure deformation.[68] Then, two parallel walls were constructed on top of the microstructure array (Figure 4C). Thus, liquids spontaneously flow through the wall channel due to capillary force, while liquid spreading is prevented by the triply reentrant profile. Three different types of channels were designed and fabricated, and the directional liquid flow along the parallel walls was visualized by fluorescence microscopy. Considering the design flexibility of TPL, it is foreseeable that more complex structures and functions, such as microfluidic platforms and lab-on-a-chip devices, can be realized by using the same principle.

## 5. Outlook

With the progressive development of 3D microprinting, it has been playing an increasingly important role in 3D microfabrication. Only very recently, its application in the field of liquid super-repellent surfaces actively started. Being a nascent research field, it has already attracted a lot of interest in different research fields. As shown in this review, the design flexibility of TPL unleashes the imagination of scientists, enabling the development of various novel 3D super-repellent microstructures with superior performances and completely new

functionalities. Despite these advances, several critical issues exist that serve as both limitations and opportunities for future development in this field. We will discuss these issues from different perspectives including technology, material, design, and application.

Due to its point-by-point writing nature, the scalability of TPL is a critical issue for large-scale applications of liquid super-repellent surfaces. To increase the throughput, parallel printing strategies by using multi-laser foci[80,107] or femtosecond projection[43,78] have been developed, which increase the printing rates up to several orders of magnitude. For both approaches, however, the laser power and cost increase with the printing speed, which ultimately limits their further progress. To go beyond that to more dramatic print-speed improvements, radically new approaches are needed. A promising direction is the light-sheet microscopy-inspired 3D-printing approach, which employs two intersecting light beams of different wavelengths to solidify localized regions.[79] Such a process does not require two-photon absorption as in TPL, but instead uses two successive one-photon absorption, therefore, enabling a reduction in the laser power and cost by 2–3 orders of magnitude. Encouragingly, such a light-sheet 3D microprinting method has recently been realized, opening a door to the next-generation high-speed 3D microprinting.[40,41]

Although mechanical robustness is essential for the applications of super-repellent 3D microstructures, this aspect has rarely been investigated. Considering that most TPL-printed microstructures are fabricated on a substrate (e.g., a glass or silicon wafer), even a partial detachment of these elements can lead to Cassie-to-Wenzel transition and the loss of liquid repellency. A common practice to improve substrate adhesion is by increasing the base diameter of the microstructures, while at the expense of increased fabrication volume and time.[81,97] A more effective method is to use the 3D-printed microstructures as a master, followed by molding and replication to create an integrated and entirely compliant super-repellent surface.[108] Nevertheless, such a molding approach comprises the design flexibility of 3D microprinting. Another interesting strategy to achieve mechanical robustness is by designing a self-compensating surface, where the underlying DRT pillars follow a bi-Gaussian stratified height distribution. When the taller ones are mechanically damaged, the shorter ones will automatically inherit the repelling roles, therefore enabling sustained liquid repellency.[109]

As exemplified by nature, super-repellent surfaces favor a hierarchically organized micro/nanostructure to attain both low adhesion and high robustness.[110–112] Although two-beam TPL has been developed to enable a feature size of 9 nm,[45] direct printing of such nanoscale features is currently still impractical. Even with the highest printing speed available ($10^7$ voxels s$^{-1}$),[80] it would take more than 100 days to fabricate a $1 \times 1 \times 0.1$ mm$^3$ surface with 10 nm resolution. Such a limitation can be potentially circumvented by a clever combination of top-down 3D printing with bottom-up self-assembly.[113,114] Recent developments in this direction have enabled the 3D printing of complex architectures with inherently nanoporous structures.[113–117] By further exploiting the rich knowledge in the field of self-assembly,[118] it is foreseeable that more advanced hierarchical liquid super-repellent structure can be realized,

where the microscale topography is defined by 3D printing and the nanoscale feature is controlled by self-assembly.

Another challenge is the development of dynamic materials to achieve adaptive liquid repellency. Till now, most of the 3D-printed liquid super-repellent microstructures are based on static materials with limited response. If the shape of these microstructures can be transformed in a controllable fashion upon an external stimulus, many new functionalities and applications could emerge including droplet transportation, rewritable liquid patterning, sensing, and encryption. Indeed, 3D printing of adaptive objects, also referred to as "4D printing", has recently become a hot research area.[119] Various types of responsive materials, including hydrogels, liquid crystalline, and composite materials, have successfully been developed for 4D microprinting, which can adapt their shape upon an external stimulus like temperature, light, pH, or magnetic and electric fields.[120–123] For printing adaptive liquid super-repellent microstructures, however, one needs to consider that the stiffness of the material must be strong enough to suspend liquids without deformation. In addition, a remote, spatially controlled response is highly desirable to enable more freedom in the design and actuation of the microstructures.

Although the performance of liquid super-repellent surfaces has improved by designing novel microstructures, the reported studies only aimed at optimizing one specific wetting property. In real applications, different properties, such as contact angle, liquid adhesion, breakthrough pressure, and mechanical reliability, need to be considered simultaneously. As these properties are antagonistically coupled, a multifaceted approach is critical to achieving an optimal design for each specific application. An early attempt in this direction has been made toward membrane distillation and droplet-based microfluidics applications, which is realized by developing an application-specific scoring function that grades a candidate design against the desired wetting properties.[124] Combining multifaceted design strategies with the power of 3D microprinting will facilitate the application of liquid super-repellent surfaces in different fields requiring distinct properties.

While most studies focus on liquid repellency in air, studying superwetting behaviors in other media like water or oil is not only important for understanding complex multiphase phenomena but also crucial for many technical applications such as emulsification,[125] foaming,[126] and gas evolution/adsorption reactions.[127] The poor side-repellency of DRT microstructures, in this case, can assist the penetration of liquid to establish a new under-liquid Cassie state. Interestingly, DRT arrays have demonstrated the unique ability to repel both air bubbles and liquid droplets in the air, underwater, and under oil.[97] Nevertheless, systematic theories for the under-liquid wetting phenomenon are still lacking, and most theoretical analyses are based on the experience of wetting research in an air environment. With its design freedom and well-defined geometrical feature, TPL provides an ideal tool to perform systematic studies on the under-liquid superwetting phenomenon.

Overall, in the past few years, significant progress in the development of super-repellent surfaces has been achieved by 3D microprinting. To move a further step toward real-world applications, multidisciplinary research involving mechanical engineering, material science, physical chemistry, computational science, and biotechnology is highly anticipated. We believe that with the rapid development both in printing technology and materials, 3D microprinting technologies will make a great impact on the development of super-repellent surfaces and extreme wettability, opening new possibilities in a myriad of applications involving solid–liquid interactions.

## Supporting Information

Supporting Information is available from the Wiley Online Library or from the author.

## Acknowledgements

## Conflict of Interest

The authors declare no conflict of interest.

## Keywords

[1] F. Yu, D. Wang, J. Yang, W. Zhang, X. Deng, *Acc. Mater. Res.* **2021**, *2*, 920.

[2] S. Pan, R. Guo, M. Björnmalm, J. J. Richardson, L. Li, C. Peng, N. Bertleff-Zieschang, W. Xu, J. Jiang, F. Caruso, *Nat. Mater.* **2018**, *17*, 1040.

[3] X. Tian, T. Verho, R. H. A. Ras, *Science* **2016**, *352*, 142.

[4] Y. Lu, S. Sathasivam, J. Song, C. R. Crick, C. J. Carmalt, I. P. Parkin, *Science* **2015**, *347*, 1132.

[5] J. W. Gose, K. Golovin, M. Boban, J. M. Mabry, A. Tuteja, M. Perlin, S. L. Ceccio, *J. Fluid Mech.* **2018**, *845*, 560.

[6] H. He, Z. Guo, *iScience* **2021**, *24*, 103357.

[7] V. Jokinen, E. Kankuri, S. Hoshian, S. Franssila, R. H. A. Ras, *Adv. Mater.* **2018**, *30*, 1705104.

[8] F. Geyer, M. D'Acunzi, C.-Y. Yang, M. Müller, P. Baumli, A. Kaltbeitzel, V. Mailänder, N. Encinas, D. Vollmer, H.-J. Butt, *Adv. Mater.* **2019**, *31*, 1801324.

[9] T. Zhu, Y. Ni, K. Zhao, J. Huang, Y. Cheng, M. Ge, C. Park, Y. Lai, *ACS Nano* **2022**, *16*, 18018.

[10] D. Wang, Q. Sun, M. J. Hokkanen, C. Zhang, F.-Y. Lin, Q. Liu, S.-P. Zhu, T. Zhou, Q. Chang, B. He, Q. Zhou, L. Chen, Z. Wang, R. H. A. Ras, X. Deng, *Nature* **2020**, *582*, 55.

**ADVANCED
SCIENCE NEWS**

www.advancedsciencenews.com

**ADVANCED
FUNCTIONAL
MATERIALS**

www.afm-journal.de

[11] Z. Dong, M. Vuckovac, W. Cui, Q. Zhou, R. H. A. Ras, P. A. Levkin, *Adv. Mater.* **2021**, *33*, 2106068.

[12] F. Piscitelli, A. Chiariello, D. Dabkowski, G. Corraro, F. Marra, L. Di Palma, *Aerospace* **2020**, *7*, 2.

[13] E. J. Falde, S. T. Yohe, Y. L. Colson, M. W. Grinstaff, *Biomaterials* **2016**, *104*, 87.

[14] H. Yong, Z. Li, X. Huang, K. Wang, Y.-N. Zhou, Q. Li, J. Shi, M. Liu, D. Zhou, *Adv. Mater. Interfaces* **2022**, *9*, 2200435.

[15] S. Wang, K. Liu, X. Yao, L. Jiang, *Chem. Rev.* **2015**, *115*, 8230.

[16] M. Liu, S. Wang, L. Jiang, *Nat. Rev. Mater.* **2017**, *2*, 17036.

[17] K. Liu, Y. Tian, L. Jiang, *Prog. Mater. Sci.* **2013**, *58*, 503.

[18] W. Barthlott, C. Neinhuis, *Planta* **1997**, *202*, 1.

[19] X.-M. Li, D. Reinhoudt, M. Crego-Calama, *Chem. Soc. Rev.* **2007**, *36*, 1350.

[20] I. S. Bayer, *Adv. Mater. Interfaces* **2020**, *7*, 2000095.

[21] Q. Zeng, H. Zhou, J. Huang, Z. Guo, *Nanoscale* **2021**, *13*, 11734.

[22] R. Hensel, C. Neinhuis, C. Werner, *Chem. Soc. Rev.* **2016**, *45*, 323.

[23] A. Tuteja, W. Choi, M. Ma, J. M. Mabry, S. A. Mazzella, G. C. Rutledge, G. H. McKinley, R. E. Cohen, *Science* **2007**, *318*, 1618.

[24] R. Hensel, R. Helbig, S. Aland, H.-G. Braun, A. Voigt, C. Neinhuis, C. Werner, *Langmuir* **2013**, *29*, 1100.

[25] T. L. Liu, C.-J. C. J. Kim, *Science* **2014**, *346*, 1096.

[26] E. M. Domingues, S. Arunachalam, J. Nauruzbayeva, H. Mishra, *Nat. Commun.* **2018**, *9*, 3606.

[27] E. M. Domingues, S. Arunachalam, H. Mishra, *ACS Appl. Mater. Interfaces* **2017**, *9*, 21532.

[28] M. Kadic, G. W. Milton, M. van Hecke, M. Wegener, *Nat. Rev. Phys.* **2019**, *1*, 198.

[29] H. Liu, H. Zhang, W. Han, H. Lin, R. Li, J. Zhu, W. Huang, *Adv. Mater.* **2021**, *33*, 2004782.

[30] T. J. Wallin, J. Pikul, R. F. Shepherd, *Nat. Rev. Mater.* **2018**, *3*, 84.

[31] C. Panwisawas, Y. T. Tang, R. C. Reed, *Nat. Commun.* **2020**, *11*, 2327.

[32] T. Li, J. Chang, Y. Zhu, C. Wu, *Adv. Healthcare Mater.* **2020**, *9*, 2000208.

[33] A. Reiser, M. Lindén, P. Rohner, A. Marchand, H. Galinski, A. S. Sologubenko, J. M. Wheeler, R. Zenobi, D. Poulikakos, R. Spolenak, *Nat. Commun.* **2019**, *10*, 1853.

[34] J. Schneider, P. Rohner, D. Thureja, M. Schmid, P. Galliker, D. Poulikakos, *Adv. Funct. Mater.* **2016**, *26*, 833.

[35] L. Keller, M. Huth, *Beilstein J. Nanotechnol.* **2018**, *9*, 2581.

[36] J. D. Fowlkes, R. Winkler, B. B. Lewis, A. Fernández-Pacheco, L. Skoric, D. Sanz-Hernández, M. G. Stanford, E. Mutunga, P. D. Rack, H. Plank, *ACS Appl. Nano Mater.* **2018**, *1*, 1028.

[37] C. Sun, N. Fang, D. M. Wu, X. Zhang, *Sens. Actuators, A* **2005**, *121*, 113.

[38] Q. Ge, Z. Li, Z. Wang, K. Kowsari, W. Zhang, X. He, J. Zhou, N. X. Fang, *Int. J. Extreme Manuf.* **2020**, *2*, 022004.

[39] M. Farsari, B. N. Chichkov, *Nat. Photonics* **2009**, *3*, 450.

[40] V. Hahn, T. Messer, N. M. Bojanowski, E. R. Curticean, I. Wacker, R. R. Schröder, E. Blasco, M. Wegener, *Nat. Photonics* **2021**, *15*, 932.

[41] V. Hahn, P. Rietz, F. Hermann, P. Müller, C. Barner-Kowollik, T. Schlöder, W. Wenzel, E. Blasco, M. Wegener, *Nat. Photonics* **2022**, *16*, 784.

[42] L. Zheng, K. Kurselis, A. El-Tamer, U. Hinze, C. Reinhardt, L. Overmeyer, B. Chichkov, *Nanoscale Res. Lett.* **2019**, *14*, 134.

[43] S. K. Saha, D. Wang, V. H. Nguyen, Y. Chang, J. S. Oakdale, S.-C. Chen, *Science* **2019**, *366*, 105.

[44] M. Carlotti, V. Mattoli, *Small* **2019**, *15*, 1902687.

[45] Z. Gan, Y. Cao, R. A. Evans, M. Gu, *Nat. Commun.* **2013**, *4*, 2061.

[46] Y. Chen, R. K. Kupka, F. Rousseaux, F. Carcenac, D. Decanini, M. F. Ravet, H. Launois, *J. Vac. Sci. Technol., B: Microelectron. Nanometer Struct.– Process., Meas., Phenom.* **1994**, *12*, 3959.

[47] C. K. Malek, V. Saile, *Microelectron. J.* **2004**, *35*, 131.

[48] R. K. Kupka, F. Bouamrane, C. Cremers, S. Megtert, *Appl. Surf. Sci.* **2000**, *164*, 97.

[49] M. Volatier, D. Duchesne, R. Morandotti, R. Arès, V. Aimez, *Nanotechnology* **2010**, *21*, 134014.

[50] M. Huff, *Micromachines* **2021**, *12*, 991.

[51] D. J. Guckenberger, T. E. de Groot, A. M. D. Wan, D. J. Beebe, E. W. K. Young, *Lab Chip* **2015**, *15*, 2364.

[52] N. Chen, H. N. Li, J. Wu, Z. Li, L. Li, G. Liu, N. He, *Int. J. Mach. Tools Manuf.* **2021**, *160*, 103670.

[53] M. A. Câmara, J. C. C. Rubio, A. M. Abrão, J. P. Davim, *J. Mater. Sci. Nanotechnol.* **2012**, *28*, 673.

[54] M. Garcia-Lechuga, O. Utéza, N. Sanner, D. Grojo, *Opt. Lett.* **2020**, *45*, 952.

[55] M. J. Pfeifenberger, M. Mangang, S. Wurster, J. Reiser, A. Hohenwarter, W. Pfleging, D. Kiener, R. Pippan, *Mater. Des.* **2017**, *121*, 109.

[56] G. Račiukaitis, *IEEE J. Sel. Top. Quantum Electron.* **2021**, *27*, 1100112.

[57] J.-F. Xing, M.-L. Zheng, X.-M. Duan, *Chem. Soc. Rev.* **2015**, *44*, 5031.

[58] Y. Lin, J. Xu, *Adv. Opt. Mater.* **2018**, *6*, 1701359.

[59] J. Song, C. Michas, C. S. Chen, A. E. White, M. W. Grinstaff, *Adv. Healthcare Mater.* **2020**, *9*, 1901217.

[60] Y. Liang, M. Frederik, H. F. B. Uwe, B. Eva, W. Martin, *Light: Adv. Manuf.* **2021**, *2*, 296.

[61] T. Young, *Philos. Trans. R. Soc. Lond.* **1805**, *95*, 65.

[62] T. Nishino, M. Meguro, K. Nakamae, M. Matsushita, Y. Ueda, *Langmuir* **1999**, *15*, 4321.

[63] R. N. Wenzel, *Ind. Eng. Chem.* **1936**, *28*, 988.

[64] A. B. D. Cassie, S. Baxter, *Trans. Faraday Soc.* **1944**, *40*, 546.

[65] A. Lafuma, D. Quéré, *Nat. Mater.* **2003**, *2*, 457.

[66] A. Tuteja, W. Choi, M. Ma, J. M. Mabry, S. A. Mazzella, G. C. Rutledge, G. H. McKinley, R. E. J. S. Cohen, *Science* **2007**, *318*, 1618.

[67] F.-M. Chang, S.-J. Hong, Y.-J. Sheng, H.-K. Tsao, *J. Phys. Chem. C* **2010**, *114*, 1615.

[68] X. Liu, H. Gu, M. Wang, X. Du, B. Gao, A. Elbaz, L. Sun, J. Liao, P. Xiao, Z. Gu, *Adv. Mater.* **2018**, *30*, 1800103.

[69] K. Koch, B. Bhushan, Y. C. Jung, W. Barthlott, *Soft Matter* **2009**, *5*, 1386.

[70] H.-J. Butt, D. Vollmer, P. Papadopoulos, *Adv. Colloid Interface Sci.* **2015**, *222*, 104.

[71] W. Choi, A. Tuteja, J. M. Mabry, R. E. Cohen, G. H. McKinley, *J. Colloid Interface Sci.* **2009**, *339*, 208.

[72] C. Dorrer, J. Rühe, *Adv. Mater.* **2008**, *20*, 159.

[73] V. Liimatainen, M. Vuckovac, V. Jokinen, V. Sariola, M. J. Hokkanen, Q. Zhou, R. H. A. Ras, *Nat. Commun.* **2017**, *8*, 1798.

[74] X. Liu, H. Gu, H. Ding, X. Du, Z. He, L. Sun, J. Liao, P. Xiao, Z. Gu, *Small* **2019**, *15*, 1902360.

[75] X. Deng, L. Mammen, H.-J. Butt, D. J. S. Vollmer, *Science* **2012**, *335*, 67.

[76] X. Zhou, J. Liu, W. Liu, W. Steffen, H.-J. Butt, *Adv. Mater.* **2022**, *34*, 2107901.

[77] J. Wei, B. Li, N. Tian, J. Zhang, W. Liang, J. Zhang, *Adv. Funct. Mater.* **2022**, *32*, 2206014.

[78] P. Somers, Z. Liang, J. E. Johnson, B. W. Boudouris, L. Pan, X. Xu, *Light: Sci. Appl.* **2021**, *10*, 199.

[79] V. Hahn, F. Mayer, M. Thiel, M. Wegener, *Opt. Photonics News* **2019**, *30*, 28.

[80] V. Hahn, P. Kiefer, T. Frenzel, J. Qu, E. Blasco, C. Barner-Kowollik, M. Wegener, *Adv. Funct. Mater.* **2020**, *30*, 1907795.

[81] Z. Dong, M. F. Schumann, M. J. Hokkanen, B. Chang, A. Welle, Q. Zhou, R. H. A. Ras, Z. Xu, M. Wegener, P. A. Levkin, *Adv. Mater.* **2018**, *30*, 1803890.

**ADVANCED
SCIENCE NEWS**

www.advancedsciencenews.com

**ADVANCED
FUNCTIONAL
MATERIALS**

www.afm-journal.de

[82] J. Sun, P. Zhu, X. Yan, C. Zhang, Y. Jin, X. Chen, Z. Wang, *Appl. Phys. Rev.* **2021**, *8*, 031403.

[83] S. Hu, X. Cao, T. Reddyhoff, D. Puhan, S.-C. Vladescu, J. Wang, X. Shi, Z. Peng, A. J. deMello, D. Dini, *Sci. Adv.* **2020**, *6*, eaba9721.

[84] R. Das, Z. Ahmad, J. Nauruzbayeva, H. Mishra, *Sci. Rep.* **2020**, *10*, 7934.

[85] D. Daniel, J. V. I. Timonen, R. Li, S. J. Velling, J. Aizenberg, *Nat. Phys.* **2017**, *13*, 1020.

[86] T.-S. Wong, S. H. Kang, S. K. Y. Tang, E. J. Smythe, B. D. Hatton, A. Grinthal, J. Aizenberg, *Nature* **2011**, *477*, 443.

[87] Q. David, *Rep. Prog. Phys.* **2005**, *68*, 2495.

[88] A. Lafuma, D. Quéré, *Europhys. Lett.* **2011**, *96*, 56001.

[89] J. D. Smith, R. Dhiman, K. Varanasi, presented at 64th Annual Meeting of the APS Division of Fluid Dynamics, Baltimore, MD November **2011**.

[90] T. Vasileiou, J. Gerber, J. Prautzsch, T. M. Schutzius, D. Poulikakos, *Proc. Natl. Acad. Sci. U. S. A.* **2016**, *113*, 13307.

[91] P. B. Weisensee, J. Tian, N. Miljkovic, W. P. King, *Sci. Rep.* **2016**, *6*, 30328.

[92] T. Vasileiou, T. M. Schutzius, D. Poulikakos, *Langmuir* **2017**, *33*, 6708.

[93] Y. Shen, X. Wu, J. Tao, C. Zhu, Y. Lai, Z. Chen, *Prog. Mater. Sci.* **2019**, *103*, 509.

[94] Z. He, M. I. Jamil, T. Li, Q. Zhang, *Langmuir* **2022**, *38*, 18.

[95] S. R. Gonzalez-Avila, D. M. Nguyen, S. Arunachalam, E. M. Domingues, H. Mishra, C.-D. Ohl, *Sci. Adv.* **2020**, *6*, eaax6192.

[96] R. Dufour, M. Harnois, V. Thomy, R. Boukherroub, V. Senez, *Soft Matter* **2011**, *7*, 9380.

[97] X. Liu, H. Gu, H. Ding, X. Du, M. Wei, Q. Chen, Z. Gu, *Adv. Sci.* **2020**, *7*, 2000878.

[98] C. B. Dayan, S. Chun, N. Krishna-Subbaiah, D.-M. Drotlef, M. B. Akolpoglu, M. Sitti, *Adv. Mater.* **2021**, *33*, 2103826.

[99] A. Chunder, K. Etcheverry, G. Londe, H. J. Cho, L. Zhai, *Colloids Surf., A* **2009**, *333*, 187.

[100] L. Ma, J. Wang, J. He, Y. Yao, X. Zhu, L. Peng, J. Yang, X. Liu, M. Qu, *ACS Appl. Mater. Interfaces* **2021**, *13*, 31285.

[101] S. Ben, T. Zhou, H. Ma, J. Yao, Y. Ning, D. Tian, K. Liu, L. Jiang, *Adv. Sci.* **2019**, *6*, 1900834.

[102] J.-J. Li, Y.-N. Zhou, Z.-H. Luo, *Prog. Polym. Sci.* **2018**, *87*, 1.

[103] L. Heepe, S. N. Gorb, *Annu. Rev. Mater. Res.* **2014**, *44*, 173.

[104] H. Li, A. J. Steckl, *Anal. Chem.* **2019**, *91*, 352.

[105] E. Berthier, A. M. Dostie, U. N. Lee, J. Berthier, A. B. Theberge, *Anal. Chem.* **2019**, *91*, 8739.

[106] Q. Zhang, S. Feng, L. Lin, S. Mao, J.-M. Lin, *Chem. Soc. Rev.* **2021**, *50*, 5333.

[107] S. Matsuo, S. Juodkazis, H. Misawa, *Appl. Phys. A* **2005**, *80*, 683.

[108] V. Liimatainen, D.-M. Drotlef, D. Son, M. Sitti, *Adv. Mater.* **2020**, *32*, 2000497.

[109] S. Hu, X. Cao, T. Reddyhoff, D. Puhan, S.-C. Vladescu, Q. Wang, X. Shi, Z. Peng, A. J. deMello, D. Dini, *ACS Appl. Mater. Interfaces* **2020**, *12*, 4174.

[110] W. Li, A. Amirfazli, *Soft Matter* **2008**, *4*, 462.

[111] A. K. Kota, J. M. Mabry, A. Tuteja, *Surf. Innovations* **2013**, *1*, 71.

[112] H. Teisala, H.-J. Butt, *Langmuir* **2019**, *35*, 10689.

[113] D. G. Moore, L. Barbera, K. Masania, A. R. Studart, *Nat. Mater.* **2020**, *19*, 212.

[114] Z. Dong, H. Cui, H. Zhang, F. Wang, X. Zhan, F. Mayer, B. Nestler, M. Wegener, P. A. Levkin, *Nat. Commun.* **2021**, *12*, 247.

[115] F. Mayer, D. Ryklin, I. Wacker, R. Curticean, M. Čalkovský, A. Niemeyer, Z. Dong, P. A. Levkin, D. Gerthsen, R. R. Schröder, M. Wegener, *Adv. Mater.* **2020**, *32*, 2002044.

[116] E. S. Farrell, Y. Schilt, M. Y. Moshkovitz, Y. Levi-Kalisman, U. Raviv, S. Magdassi, *Nano Lett.* **2020**, *20*, 6598.

[117] J. Monti, A. Concellón, R. Dong, M. Simmler, A. Münchinger, C. Huck, P. Tegeder, H. Nirschl, M. Wegener, C. O. Osuji, E. Blasco, *ACS Appl. Mater. Interfaces* **2022**, *14*, 33746.

[118] L. Cademartiri, K. J. M. Bishop, *Nat. Mater.* **2015**, *14*, 2.

[119] C. A. Spiegel, M. Hippler, A. Münchinger, M. Bastmeyer, C. Barner-Kowollik, M. Wegener, E. Blasco, *Adv. Funct. Mater.* **2020**, *30*, 1907615.

[120] M. Hippler, E. Blasco, J. Qu, M. Tanaka, C. Barner-Kowollik, M. Wegener, M. Bastmeyer, *Nat. Commun.* **2019**, *10*, 232.

[121] D. Jin, Q. Chen, T.-Y. Huang, J. Huang, L. Zhang, H. Duan, *Mater. Today* **2020**, *32*, 19.

[122] H. Zeng, P. Wasylczyk, C. Parmeggiani, D. Martella, M. Burresi, D. S. Wiersma, *Adv. Mater.* **2015**, *27*, 3883.

[123] C. Peters, M. Hoop, S. Pané, B. J. Nelson, C. Hierold, *Adv. Mater.* **2016**, *28*, 533.

[124] J. Panter, Y. Gizaw, H. J. S. a. Kusumaatmaja, *Sci. Adv.* **2019**, *5*, eaav7328.

[125] C. Chen, D. Weng, A. Mahmood, S. Chen, J. Wang, *ACS Appl. Mater. Interfaces* **2019**, *11*, 11006.

[126] W. S. Y. Wong, L. Naga, L. Hauer, P. Baumli, H. Bauer, K. I. Hegner, M. D'Acunzi, A. Kaltbeitzel, H.-J. Butt, D. Vollmer, *Nat. Commun.* **2021**, *12*, 5358.

[127] Q. Zhang, M. Zhou, G. Ren, Y. Li, Y. Li, X. Du, *Nat. Commun.* **2020**, *11*, 1731.

**ADVANCED
SCIENCE NEWS**
www.advancedsciencenews.com

**ADVANCED
FUNCTIONAL
MATERIALS**
www.afm-journal.de

**Zheqin Dong** is head of the Biomedical Additive Manufacturing research group at Shandong University, China. He obtained B.S. and Ph.D. in Chemical Engineering from the East China University of Science and Technology, China, in 2012 and 2019, respectively. He then joined Dr. Pavel Levkin's group at Karlsruhe Institute of Technology (KIT) as a postdoc from 2019 to 2022. His current research focuses on 3D printing functional materials and devices for biomedical applications.

**Pavel Levkin** is head of the Multifunctional Materials Systems research group at the Karlsruhe Institute of Technology (KIT), Germany. His research focuses on the development of functional and responsive materials and surfaces for biomedical and biotechnological applications and on the miniaturization of chemical and biological experiments for drug discovery. He received the Heinz-Meyer Leibnitz Prize, Ewald-Wicke Prize as well as an ERC Starting Grant. He is also a co-founder of two biotech companies.